FOCAL PLANE ARRAY BREADBOARD FOR ADVANCED MULTIPLE BEAM RADIOMETR ANTENNAS

C. Cappellin[(1)], J. R. de Lasson [(1)], O. Iupikov[(2)], M. Ivashina[(2)], N. Skou[(3)], K. Pontoppidan[(1)], B. Fiorelli[(4)]

[(1)] TICRA, Landemærket 29, DK 1119 Copenhagen, Denmark, Email: cc@ticra.com, jrdl@ticra.com, kp@ticra.com
[(2)] Chalmers University of Technology, SE-412 96 Gothenburg, Sweden, Email: oleg.iupikov@chalmers.se, marianna.ivashina@chalmers.se
[(3)]National Space Institute, Technical University of Denmark, DK 2800 Lyngby, Denmark, Email: ns@space.dtu.dk
[(4)]ESA/STEC, Keplerlaan 1, 2201 AZ Noordwijk, The Netherlands, Email: benedetta.fiorelli@esa.int

***Abstract* – The detailed design and RF analysis of a breadboard made by 35 x-polarized and 32 y-polarized Vivaldi antennas, placed 0.67 wavelength from each other and located above a finite ground plane, are described. The breadboard constitutes a representative part of the feed array illuminating a conical scan or push-broom antenna for next generation microwave radiometers for ocean observation. The analysis are done at 6.9 GHz including mutual coupling between the elements, and in two commercial software, i.e. CST and the MoM add-on to GRASP.**

I. INTRODUCTION

Next generation microwave radiometers for ocean observation will need to deliver high spatial and radiometric resolution Sea Surface Temperature (SST) and vector wind fields, with the highest possible absolute accuracy and closer to coasts and sea ice than seen hitherto, see the requirements of Table 1, similar to the ones considered by MICROWAT and addressed in [1] and [2]. There is also an interest in combining SST measurements in C band with ocean salinity measurements done in L band.

Table 1: Radiometric requirements for next generation SST and wind fields observations.

Frequencies [GHz]	Pol	ΔT [K]	Accuracy [K]	Footprint [km]	Distance to coast/ice [km]
C band: 6.9 ± 0.1 7.3 ± 0.1	V and H	0.3	0.25	20	15-20

Current spaceborne microwave radiometers for SST and wind fields operating in C-band, like AMSR-2 and WindSat for example [3]-[4], provide a spatial resolution, defined as the 3-dB footprint, of around 55 km, whereas less than 20 km is desirable. The radiometric resolution in C band for WindSat is around 0.7 K, while 0.3 K is needed. Moreover, current systems provide measurements not closer than around 100 km from the shore-line, because of the signal contamination provided by the antenna side-lobes illuminating the land, significantly warmer than the sea. There is a strong desire to reduce this distance to 5-15 km.
While the spatial resolution of Table 1 can be achieved by correctly sizing the reflector antenna aperture, i.e. 5 m, the required radiometric resolution can only be met by considering several simultaneous beams in the along- and across-track, either in a push-broom system, or in a multi-beam scanning system, see Figure 1.

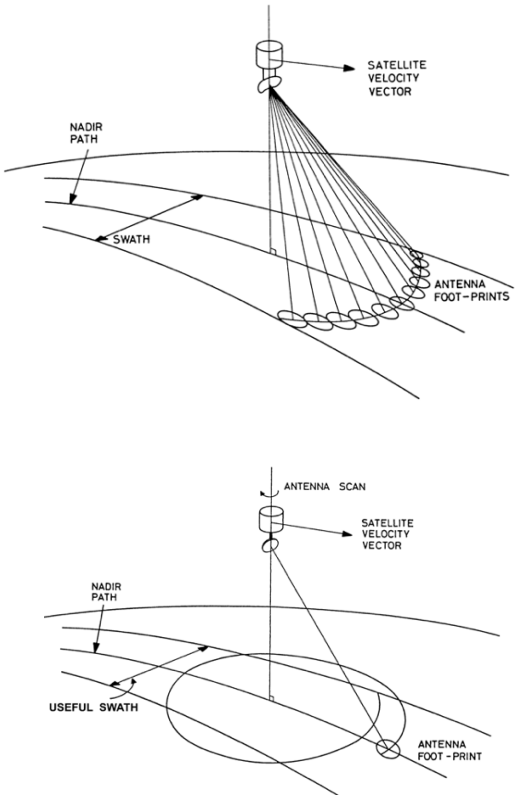

Figure 1: Push-broom (top) and scanning (bottom) antenna systems for the radiometer under study.

The push-broom system achieves very high radiometric resolution since all across track footprints are measured simultaneously by their own receivers [5]. It was shown

in [1] that the radiometric resolution of the push-broom system is one order of magnitude higher than the one of a conical scan with same projected aperture. The push-broom antenna has the clear advantage of being stationary, but the number of beams to cover the swath can be large, and requires a large torus reflector and a correspondingly large feed array. The multi-beam scanning system achieves high radiometric resolution by measuring each footprint several times followed by integration. The antenna is slightly smaller than an equivalent torus, needs a smaller feed array, but presents numerous challenges in order to achieve a well-balanced rotation at satellite level [6], which has been solved in the US for SMAP but which is not directly available in Europe yet.

In the ESA contract 4000107369-12-NL-MH run between 2013-2015 it was shown that both types of antenna systems could meet the challenging requirements of Table 1, provided the reflector antennas were illuminated by a focal plane array of closely spaced elements, properly excited and controlled by a digital beam former, see [2] and Figure 2. More elements take part in the formation of each beam and the same element takes part in the formation of multiple beams. The chosen array element was a half wave dipole above an infinite ground plane, and mutual coupling between the elements was disregarded, implying identical element patterns.

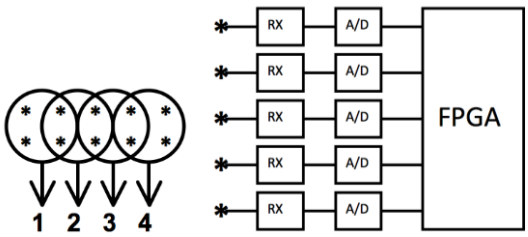

Figure 2: To the left, the array concept where the beams are indicated by (1,2,3,4) and the array elements by a star. To the right, the receiving system where each array element has its own receiver, followed by a common FPGA.

The ESA activity "Focal Plane Array Bread-Board for Advanced Multiple Beam Radiometer Antenna", contracted to TICRA with Chalmers University and DTU-Space (ESA contract 4000117841/16/NL/FF/gp) and currently ongoing, has the purpose to prove the focal plane array concept, and verify if the radiometric requirements of Table 1 can still be met with a realistic array with non-identical element patterns. The activity is divided in three phases: in the first one, a trade-off analysis of a few promising radiator candidates is performed to select the radiator type of the breadboard of the feed array. In the second one, a representative breadboard of the feed array is designed and analysed in detail with two commercial EM software, by including mutual coupling between the elements and a finite size of the array. The element patterns of the manufactured breadboard are then accurately measured and the accuracy of the computer models is thus validated. It is underlined that the detailed and accurate RF modelling of the full antenna system is indeed of paramount importance for the accurate calibration of the radiometer and represents the main goal of the ongoing study. In the third and last phase, the full array models are set up in order decsribe the full feed array for the push-broom antenna studied and designed in [2]. The individual element patterns computed in this way are then input the optimisation algorithms developed by TICRA and Chalmers in [2] and [7], and the updated radiometric performances of the push-broom antenna with non-identical element patterns are finally obtained.

This paper will describe the work done in the first two phases, up to the manufacturing. In particular, Section II and Section III briefly summarize the radiometric and antenna requirements, respectively, which can be derived from Table 1. Section IV focuses on the radiating element requirements leading to the array element chosen for the breadboard, which is described in detail in Section V. Section VI shows the detailed RF analysis of the breadboard, by comparing the element patterns of a few selected elements, as computed in the commercial software packages GRASP and CST. Finally, Section VII shows the breadboard manufactured by Chalmers University, which is currently undergoing RF test at the DTU-ESA Spherical Near-Field Facility at the Technical University of Denmark.

II. Radiometric Requirements

The radiometric requirements are contained in Table 1. It is seen that the instrument shall measure brightness temperature in two linear polarizations. A typical orbit of 817 km and an incidence angle of 53° are selected. A swath width of 1500 km is chosen for the conical scan antenna, while 600 km is used for the push-broom antenna, in order to limit the size of the torus reflector and the associated feed array. It is possible to derive that for a 5 m conical scan antenna, 2 beams along track are necessary to meet the requirements for the radiometric resolution of Table 1, see [1], with fore-and-after look and 11.5 RPM. A 5 m X 7.5 m push-broom antenna requires instead 58 beams across track.

III. Antenna Requirements

The antenna requirements can be derived from the radiometric requirements of Table 1. Besides the 5 m antenna projected aperture derived by the footprint, one additional requirement concerns the cross-polarisation of the antenna. The radiometer shall measure brightness temperatures in two linear polarisations, vertical and horizontal, and with an accuracy of 0.25 K. This is fulfilled when the cross-polar power received from the Earth does not exceed 0.29% of the total power coming

from the Earth for that polarization state in C band, see [8] for a detailed derivation.
Finally, to measure the brightness temperature of the sea when the satellite covers regions with both land and sea and if we want an accuracy of 0.25 K, the coast line must be located outside a cone of angle θ_c which contains 99.72% of the radiated power. The goal is to make this cone as narrow as possible, in order to achieve the required distance to coast, see Figure 3 and [8] for a detailed derivation.

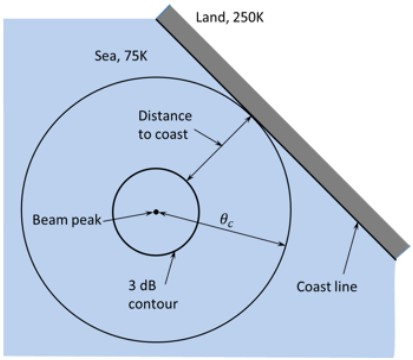

Figure 3: Schematic drawing of the distance to coast concept, showing a footprint falling on the sea near the coast.

It was derived in [1] that 35 (7 X 5) dual-polarized array elements displaced by 0.75 wavelengths on an xy-grid are necessary to generate two compliant beams in C band for the 5 m conical antenna. For the 5 m X 7.5 m push-broom antenna, the feed array is planar, but located on a rho-phi grid, see [2]: 6 X 13 dual polarized array elements are needed to generate each of the 58 beams. Since all elements take part in the formation of multiple beams, the total number of array elements in C band is 666 dual polarized elements.

IV. Radiating Element Requirements

The breadboard of the present study should not represent the full feed array necessary to produce the beams for the conical scan or push-broom antenna, but should as a minimum contain 5 X 7 elements over a finite ground plane. A list of the electrical and mechanical requirements were set up by Chalmers University in order to study possible candidates for the array element type to be used in the breadboard, as shown in Table 2. It is noted that the cross-polarization level is important for the full array when properly excited, but not for the single radiating element, for which no clear values can be defined. Finally, it is observed that there is no direct requirement for the peak directivity, though it is clear that, due to an element size smaller than a wavelength, the peak directivity will not be higher than 7-8 dBi and that the pattern will be broad. This indirectly also means that the element pattern will be sufficiently broad to illuminate the reflector within its subtended angle.

Table 2 Radiating element requirements.

Frequency	C band: 6.9 ± 0.1 & 7.3 ± 0.1 GHz
Polarization	Dual linear
Matching conditions	The amplitude of the active reflection coefficient should not exceed -10 dB for a 50 Ohm input impedance, when the element is in the final array environment and the optimum excitation coefficients are applied.
Element size	smaller than 0.75λ in both x and y
Feeding network	Single-ended output ports of the antenna elements (no baluns) are preferred.
Use of dielectric	Possibly minimized to reduce losses
Cost	The choice of the materials of the antenna elements, assembly and manufacturing should be within the budget of the project.

V. Radiating Element Design

Three antenna elements were considered as potential candidates for the array element to be used in the breadboard, namely a crossed dipole, a patch excited cup from RUAG [9] and a Vivaldi antenna [10], see Figure 4.

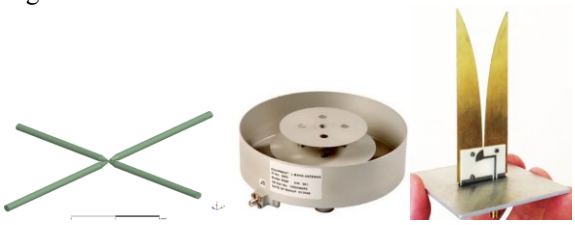

Figure 4: Candidates for the radiating element of the breadboard.

The three elements were chosen since they satisfied the majority of the requirements listed in Table 2, and their RF modelling was well-known. They however differed greatly in other aspects, i.e. the crossed dipole is just an electromagnetic model, the patch excited cup is a space qualified hardware, while the Vivaldi has only been used for on-ground applications so far. The three elements were used in a 6 x 13 array with spacing of 0.7 wavelength from each other, in order to generate one beam of the push-broom antenna. To compute the radiated field of the 6x13 array in this preliminary phase, the element patterns of the array were considered identical and were computed as the array was infinite and located above an infinite ground plane. It was found that the radiometric performances of the beam of the push-broom antenna were very similar, no matter which

antenna element was used, and that all satisfied the requirements of Table 1.

Due to lightweight properties and mechanical stiffness, cost constraints as well as broadband capabilities, the Vivaldi element was chosen for the breadboard. The element was considered the best choice from the RF modelling point of view, showing challenges in accurately modelling the PCB with microstrip, coaxial excitation and the well-defined profile.

The Vivaldi element was further designed by Chalmers University, taking as outset the Embrace antenna element (500-1500 MHz) presented in [11], and scaling it up in frequency as described in [12]. The scaled-up element geometry was re-optimized in profile and cavity size in order to achieve low active reflection coefficient. Later on, the microstrip feeding was optimized in width, stub radius and dielectric thickness, using the optimization approach in [13]. The final design I shown in Figure 5.

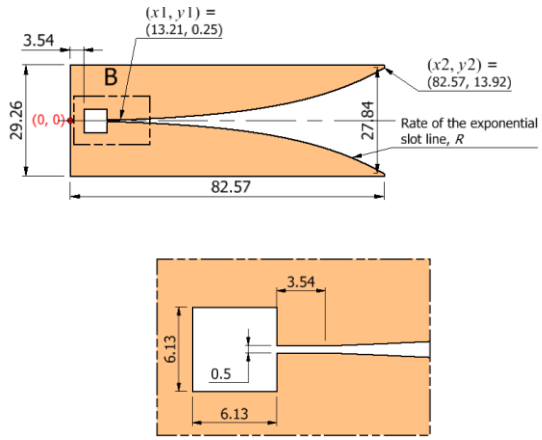

Figure 5: Detailed geometry of the Vivaldi antenna: the antenna is made of aluminum with 0.4 mm thickness.

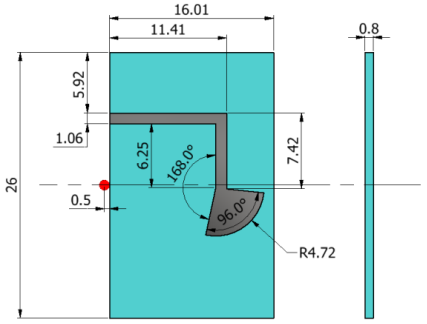

Figure 6: The feeding PCB of the Vivaldi antenna element. The dielectric material for the PCB is Rogers RO4003 with permittivity equal to 3.55 and loss tangent equal to 0.0027.

The Vivaldi element designed according to Figure 5 and Figure 6 was modelled by Chalmers University in HFSS and CST and by TICRA in the MoM add-on to GRASP, and analyzed above a finite size ground plane of 58 mm X 58 mm. Moreover, the element was manufactured by Chalmers University, see Figure 7, and the S11 spectrum was measured from 3 GHz to 8.0 GHz. Results of the computed and measured S11 are shown in Figure 8: the agreement between the curves is very good. The patterns computed by HFSS and the MoM add-on to GRASP at 6.9 GHz are shown in

Figure 9 and Figure 10, respectively, showing again exceptional agreement.

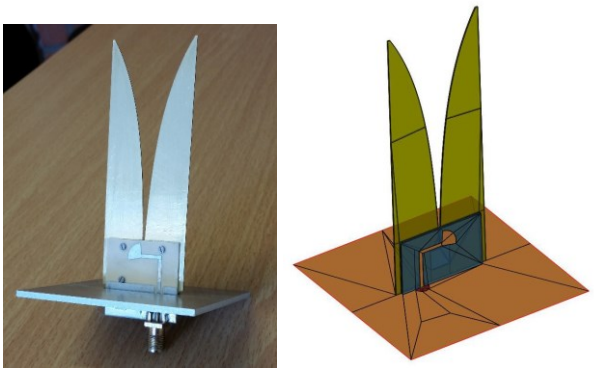

Figure 7: Manufactured Vivaldi element above a 58 mm ground plane, and MoM-mesh plot of the antenna model in GRASP: in blue the PCB slab, in transparent green the Vivaldi antenna with 0.4 mm thickness and in brown the ground plane.

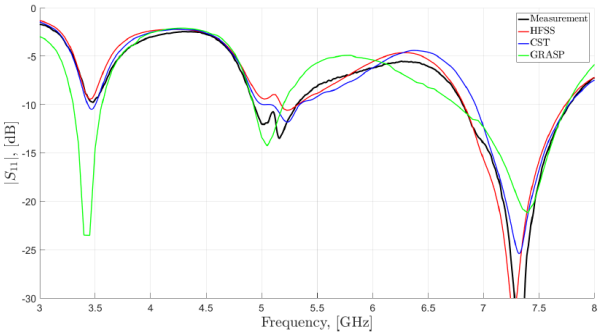

Figure 8: Computed and measured S11 over the [3:8] GHz frequency range.

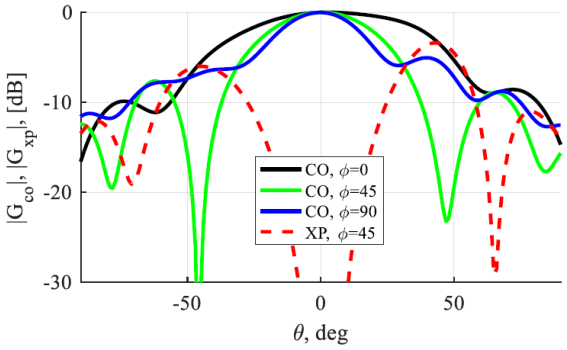

Figure 9: Co-polar and cross-polar components of the far-field pattern of Figure 7 computed by HFSS at 6.9 GHz.

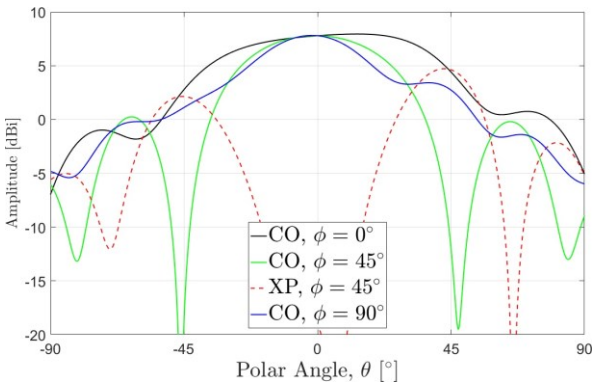

Figure 10: Co-polar and cross-polar components of the far-field pattern of Figure 7 computed by the MoM add-on to GRASP at 6.9 GHz.

VI. Detailed RF Analysis of the Breadboard

The breadboard consists of 35 x-polarized and 32 y-polarized Vivaldi antennas placed 0.67 wavelength (29.26 mm at 6.9 GHz) from each other and located on an xy-grid above a ground plane of 265 mm X 200 mm X 5 mm, as shown in Figure 11. The Vivaldi antennas are 83 mm high and 0.4 mm thick. Each Vivaldi element is excited by a coaxial waveguide with 50 Ohm characteristic impedance. This leads to 35+32= 67 SMA female connectors on the rear side of the ground plane. In addition, 26 half Vivaldi antenna elements are located at the edge of the breadboard, in direct connection to the above elements, as shown in Figure 11. These additional elements are dummy, and thus are not directly excited. Their purpose is both to reduce the edge truncation effect and to make the breadboard more stiff. Again, the MoM add-on to GRASP and CST are used to analyze the array elements radiation.

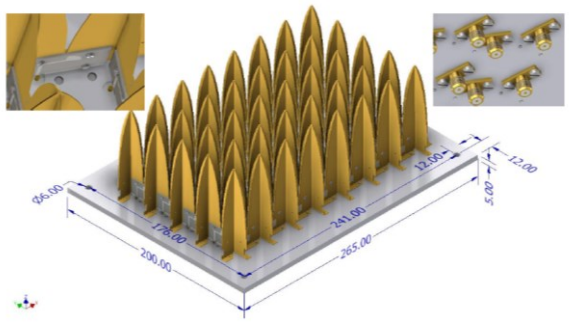

Figure 11: Mechanical drawing of the breadboard.

A. GRASP Model

The breadboard of Figure 11 was set up in the MoM add-on to GRASP by TICRA in order to compute the pattern of a few selected elements. The thickness of the Vivaldi elements and of the ground plane was disregarded, as well as the screws in the PCB slab. The GRASP model is shown in Figure 12 and details on the feeding of the Vivaldi elements are seen in Figure 13.

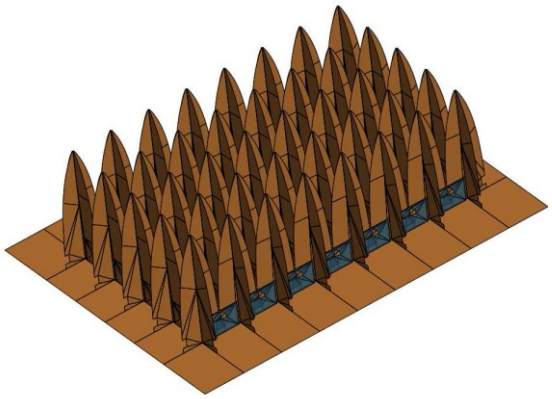

Figure 12: Model of the breadboard in the MoM add-on to GRASP. All Vivaldi elements and the finite size ground plane are visible.

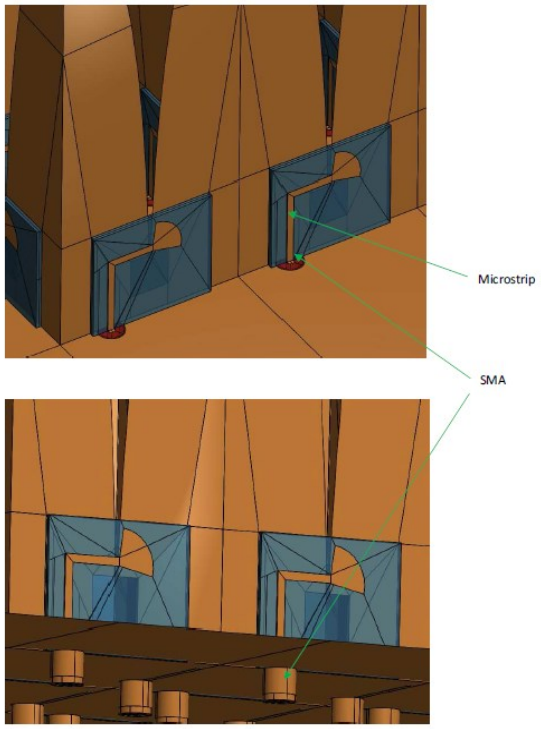

Figure 13: Model of the breadboard in the MoM add-on to GRASP: zoom in on the microstrip and port excitation.

B. CST Model

As the GRASP model of Section A, the model in CST of Chalmers was a slightly simplified version of the mechanical model. The CST model was identical to the GRASP model, a part from including the finite thickness of the Vivaldi and ground plane, see Figure 14.

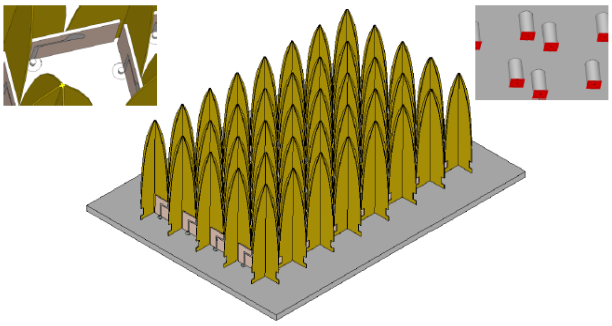

Figure 14: Model of the breadboard in CST. All Vivaldi elements and the finite size ground plane are visible, as well as details on the port excitation.

C. Comparison of GRASP and CST patterns

The models developed in GRASP and CST were thus used to compute the pattern of the array elements, where mutual coupling among all elements is included. One element is excited at a time, while the others are matched. In the following we will compare these patterns for three array elements, according to the indexing of Figure 15. All patterns refer to a coordinate system with origin at the center of the ground plane, x-axis parallel to the long side of the breadboard, and y-axis parallel to the short side of the breadboard.

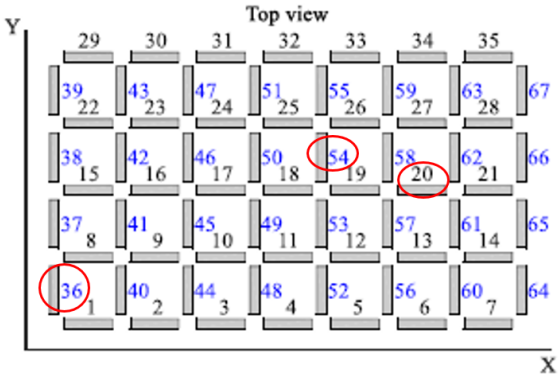

Figure 15: Array element indexing: x-oriented Vivaldi elements are written in black, while y-oriented in blue. The three elements used for pattern comparison are highlighted in red.

Element 36

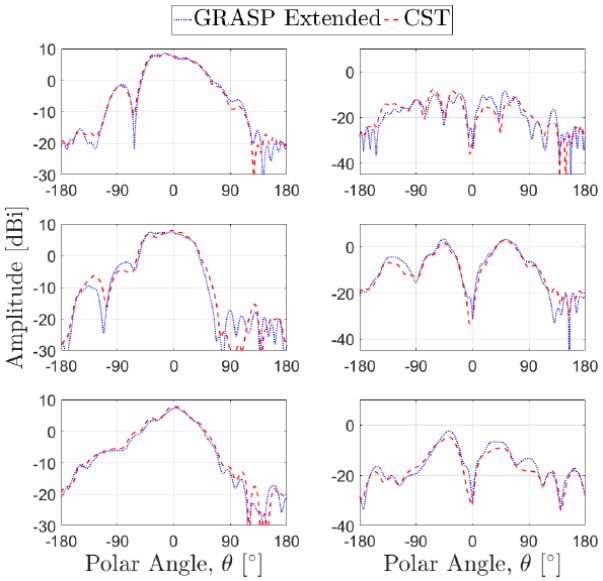

Figure 16: Pattern of the element 36: to the left the co-polar component, and to the right the cross-polar component. At the top φ=0°, in the middle φ=45°, at the bottom φ=90°.

From Figure 16 it is seen that for the corner element 36 the GRASP and CST agreement is very good. Many pattern details are equally reproduced in the co-polar and cross-polar components, on all φ cuts. The largest differences are seen in the co-polar component for $|\theta| \approx 90°$ in the φ=45° cut.

Element 54

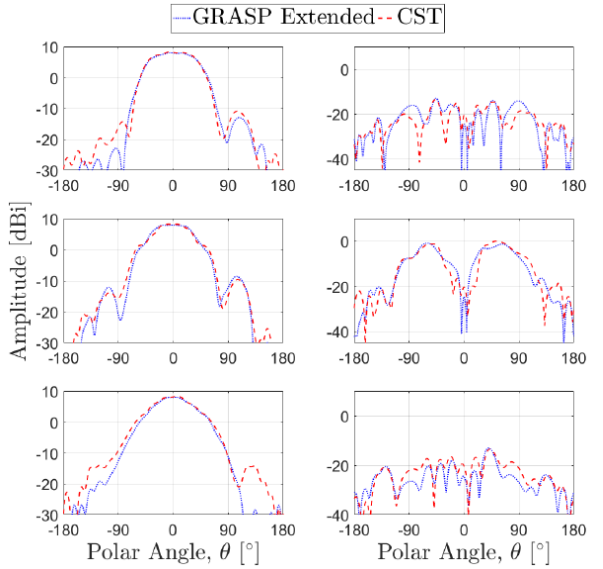

Figure 17: Pattern of the element 54: to the left the co-polar component, and to the right the cross-polar component. At the top φ=0°, in the middle φ=45°, at the bottom φ=90°.

Element 54 is located close to the center of the array. Figure 17 shows that for the co-polar component the GRASP-CST agreement is good for the peak level and pattern shape out to approximately |θ|=80°. At larger |θ| and especially for φ=90° some differences are observed in the co-polar component. The cross-polar component agrees again well, like for element 36, at the overall level and in most of the details over the full angular domain.

Element 20

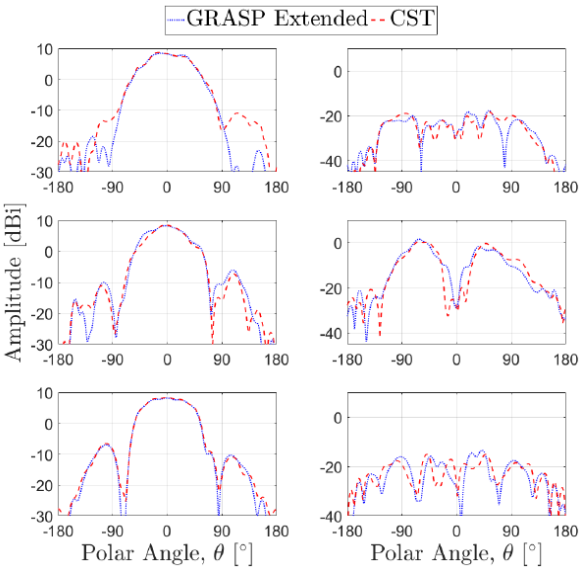

Figure 18: Pattern of the element 20: to the left the co-polar component, and to the right the cross-polar component. At the top φ=0°, in the middle φ=45°, at the bottom φ=90°.

For the x-oriented and fairly centrally located element 20, the picture is roughly as for the element 54, though with the largest disagreement for the co-polar component occurring in the φ=0° cut for |θ| > 90°. It is thus interesting to notice that for the two centrally located elements, the largest GRASP-CST disagreement between the co-polar components is seen in the cuts parallel to the orientation of the respective elements. The cross-polar component agrees again well, like for element 36 and 54, at the overall level and in most of the details over the full angular domain.

It is finally observed that the patterns of the elements in the breadboard configuration differ from the one of the single element over a small ground plane of Figure 9 and Figure 10. This clearly shows that the mutual coupling between the closely spaced elements of the breadboard is a significant effect that has to be taken into account in the detailed RF modelling.

VII. MANUFACTURING OF THE BREADBOARD

The breadboard of Figure 11 was then manufactured by Chalmers University, as shown in *Figure 19*, and shipped to Denmark, where it is currently undergoing RF test at the DTU-ESA Spherical Near-Field Antenna Test Facility at the Technical University of Denmark.

Figure 19 Breadboard manufactured at Chalmers University.

VIII. CONCLUSIONS

The detailed design and RF analysis of a breadboard made by 35 x-polarized and 32 y-polarized Vivaldi antennas, placed 0.67 wavelength from each other and located above a finite ground plane, were described. The breadboard constitutes a representative part of the feed array illuminating a 5 m conical scan or push-broom antenna for next generation microwave radiometers for ocean observation. The analysis of the breadboard were done at 6.9 GHz including mutual coupling between the elements, and in two commercial software, i.e. CST and the MoM add-on to GRASP. The results showed that the agreement in RL and pattern between the two software was excellent when considering one single Vivaldi element on a small ground plane. The agreement remained very good when comparing the patterns of three different elements of the breadboard, though a few differences were observed in the co-polar component for |θ| > 90° in the plane parallel to the orientation of the element.

IX. ACKNOWLEDGEMENTS

We would like to acknowledge RUAG Space (Johan Wettergren and Susanne Schilliger Kildal), Sweden, for providing us with the data for the patch-excited cup antenna.

X. REFERENCES

[1] C. Cappellin et al., "Novel Multi-Beam Radiometers for Accurate Ocean Surveillance", in *Proc. EuCAP Conference*, Den Haag, The Netherlands, 2014.

[2] C. Cappelin et at., "Design of Push-Broom Multi-Beam Radiometer for Future Ocean Observations", *in Proc. EuCAP Conference*, Lisbon, Portugal, 2015.

[3] P. W. Gaiser, et al., "The WindSat Spaceborne Polarimetric Microwave Radiometer: Sensor Description and Early Orbit Performance", IEEE Trans. Geo. Rem. Sensing, Vol. 42, No. 11, November 2004.

[4] http://nsidc.org/data/docs/daac/amsre_instrument.gd.html

[5] P. Nielsen, K. Pontoppidan, J. Heeboell, B. le Stradic, "Design, Manufacture and Test of a Pushbroom Radiometer", *in Proc. Ant. Prop. Conference*, ICAP 1989.

[6] M. Mobrem, E. Keay, G. Marks, E. Slimko, "Development of the large aperture reflector/boom assemby for the SMAP spacecraft", *in Proc. ESA workshop on Large Deployable Antennas*, ESA/ESTEC, Noordwijk, The Netherlands, 2012.

[7] A. Iupikov, et. al. ,"An optimal beamforming algorithm for phased-array antennas used in multi-beam spaceborne radiometers," *in Proc. EuCAP Conference*, Lisbon, Portugal, 2015.

[8] TN1, ESA contract 4000117841/16/NL/FF/gp "Focal Plane Array Bread-Board for Advanced Multiple Beam Radiometer Antenna", 2017.

[9] J. Johansson and P. Ingvarson, "Array antenna activities at RUAG space: An overview," *in Proc. EuCAP Conference*, Gothenburg, Sweden, 2013.

[10] O. A. Iupikov, A. A. Roev, and M. V. Ivashina, "Prediction of farfield pattern characteristics of phased array fed reflector antennas by modeling only a small part of the array – Case study of spaceborne radiometer antennas," *in Proc. EuCAP Conference*, Paris, France, 2017.

[11] G. W. Kant, P. D. Patel, S. J. Wijnholds, M. Ruiter, and E. van der Wal, "EMBRACE: A multi-beam 20,000-element radio astronomical phased array antenna demonstrator," IEEE Trans. Antennas Propag., vol. 59, no. 6, pp. 1990–2003, Jun. 2011.

[12] O. A. Iupikov, A. A. Roev, M. V. Ivashina, 'Prediction of Far-Field Pattern Characteristics of Phased Array Fed Reflector Antennas by Modeling Only a Small Part of the Array – Case Study of Spaceborne Radiometer Antennas', *In Proc. EuCAP Conference*, Paris, France, 2017.

[13] M. V. Ivashina, E. A. Redkina, and R. Maaskant, 'An Accurate Model of a Wide-Band Microstrip Feed for Slot Antenna Arrays', *In Proc. of IEEE International Symposium on Antennas and Propagation*, Honolulu, Hawaii, USA June 10-15, 2007.